frontiers | Frontiers in Cell and Developmental Biology

TYPE Original Research
PUBLISHED 23 May 2023
DOI 10.3389/fcell.2023.1186526

OPEN ACCESS

EDITED BY
Kunimasa Ohta,
Kyushu University, Japan

REVIEWED BY
J. Gage Crump,
University of Southern California, United States
Matthew Anderson,
National Cancer Institute at Frederick (NIH), United States

*CORRESPONDENCE
Jennifer L. Fish,
Jennifer_Fish@uml.edu

RECEIVED 14 March 2023
ACCEPTED 09 May 2023
PUBLISHED 23 May 2023

CITATION
Zbasnik N and Fish JL (2023), *Fgf8* regulates first pharyngeal arch segmentation through pouch-cleft interactions.
Front. Cell Dev. Biol. 11:1186526.
doi: 10.3389/fcell.2023.1186526

Fgf8 regulates first pharyngeal arch segmentation through pouch-cleft interactions

Nathaniel Zbasnik and Jennifer L. Fish*

Department of Biological Sciences, University of Massachusetts Lowell, Lowell, MA, United States

Introduction: The pharyngeal arches are transient developmental structures that, in vertebrates, give rise to tissues of the head and neck. A critical process underlying the specification of distinct arch derivatives is segmentation of the arches along the anterior-posterior axis. Formation of ectodermal-endodermal interfaces is a key mediator of this process, and although it is essential, mechanisms regulating the establishment of these interfaces vary between pouches and between taxa.

Methods: Here, we focus on the patterning and morphogenesis of epithelia associated with the first pharyngeal arch, the first pharyngeal pouch (pp1) and the first pharyngeal cleft (pc1), and the role of *Fgf8* dosage in these processes in the mouse model system.

Results: We find that severe reductions of *Fgf8* levels disrupt both pp1 and pc1 development. Notably, out-pocketing of pp1 is largely robust to *Fgf8* reductions, however, pp1 extension along the proximal-distal axis fails when *Fgf8* is low. Our data indicate that *Fgf8* is required for specification of regional identity in both pp1 and pc1, for localized changes in cell polarity, and for elongation and extension of both pp1 and pc1.

Discussion: Based on *Fgf8*-mediated changes in tissue relationships between pp1 and pc1, we hypothesize that extension of pp1 requires physical interaction with pc1. Overall, our data indicate a critical role for the lateral surface ectoderm in segmentation of the first pharyngeal arch that has previously been under-appreciated.

KEYWORDS

pharyngeal plate, jaw evolution, pharyngeal pouches, DiGeorge syndrome, 22q11.2, pharyngeal cleft

1 Introduction

The pharyngeal arches (PAs) are transient developmental structures that, in vertebrates, give rise to tissues of the head and neck. The PAs are formed by mesenchymal populations, the neural crest (NC) and mesoderm, that migrate in between epithelial layers, the surface ectoderm and foregut endoderm (Depew et al., 2002a). The mesenchymal cells of each arch give rise to specific musculoskeletal derivatives. For example, the jaw derives from the first pharyngeal arch (PA1), while the second arch, in mammals, forms the stapes and contributes to the hyoid bone. A critical process underlying the specification of these different skeletal elements is segmentation of the arches along the anterior-posterior axis, which ensures separation of mesenchymal populations and allows for their differential patterning (Graham and Smith, 2001). Arch segmentation is mediated by the pharyngeal epithelia. Pharyngeal

pouches form via localized out-pocketing of the foregut endoderm that grows laterally to contact the ectoderm, which invaginates to form the pharyngeal clefts (Graham, 2001; Graham, 2003; Graham et al., 2005). Mutations or experimental alterations resulting in the failure to generate pharyngeal pouches also cause failure of pharyngeal arch formation (Piotrowski and Nusslein-Volhard, 2000; Couly et al., 2002; Edlund et al., 2014).

In addition to arch segmentation, pharyngeal epithelia provide essential signals regulating the patterning and proliferation of arch mesenchyme (Trumpp et al., 1999; Couly et al., 2002; Brito et al., 2006; Haworth et al., 2007; Edlund et al., 2014; Hasten and Morrow, 2019). Subsequent to these key patterning roles, the pouches and clefts also give rise to essential tissues of the head (Grevellec and Tucker, 2010). Thus, the pharyngeal epithelia have at least 3 critical roles: 1) segmenting the arches, 2) providing signals that support patterning and proliferation of arch mesenchyme, and 3) differentiating into tissue derivatives. Given that differential patterning of each arch along the anterior-posterior axis is required for the formation of arch-specific derivatives (e,g., Gendron-Maguire et al., 1993; Rijli et al., 1993; Trainor and Krumlauf, 2001), and tissue derivatives of the pouches and clefts differ among vertebrate taxa (Grevellec and Tucker, 2010; Poopalasundaram et al., 2019), it is not surprising that arch segmentation varies between arches along the anterior-posterior axis and between the same arch in different taxa. These differences have been characterized in terms of ectodermal-endodermal tissue relationships (Shone and Graham, 2014) and molecular mechanisms of out-growth (Quinlan et al., 2002; Piotrowski et al., 2003; Crump et al., 2004; Okubo et al., 2011; Choe et al., 2013; Hasten and Morrow, 2019).

Our work investigates development of the lower jaw and how alterations to jaw development contribute to human disease. Therefore, we specifically focus on the patterning and morphogenesis of PA1 and its associated epithelia, the first pharyngeal pouch (pp1) and the first pharyngeal cleft (pc1). We previously described how *Fgf8* has a dosage effect on jaw size. Specifically, reductions in *Fgf8* expression below about 40% of WT expression levels result in truncated and dysmorphic lower jaws (Green et al., 2017; Zbasnik et al., 2022). Mild mutants ($Fgf8^{Neo/Neo}$; expressing 35% of *Fgf8* relative to WT) exhibit minor truncations of the proximal mandible whereas more severe mutants ($Fgf8^{\Delta/Neo}$; expressing 20% of *Fgf8* relative to WT) exhibit unilateral fusion of the upper and lower jaws (Zbasnik et al., 2022). Importantly, these defects are associated with malformations of PA1 epithelia which fail to separate the first and second arches. As a consequence, the expression patterns of key patterning genes are altered. Based on these data, we hypothesized that *Fgf8*-mediated morphogenesis of pharyngeal epithelia is critical to arch segmentation and PA1 patterning.

Defects in pp1 morphogenesis are associated with several craniofacial disease syndromes including DiGeorge (22q11.2 deletion) Syndrome (Jerome and Papaioannou, 2001; Frank et al., 2002; Piotrowski et al., 2003; Zhang et al., 2005; Arnold et al., 2006; Moon et al., 2006). Although human FGF8 does not localize to 22q11, *Fgf8* deficiency in mice generates many features of 22q11.2 deletion syndromes (Frank et al., 2002). Fgf8 is an important developmental signaling factor that genetically interacts with *Tbx1* and *Crkl*, two genes that lie within 22q11.2 (Vitelli et al., 2002a; Vitelli et al., 2002b; Moon et al., 2006). *Fgf8* is expressed in both pp1 and pc1 where it overlaps with *Tbx1* and *Foxi3* expression (Hasten and Morrow, 2019). Both *Tbx1* and *Foxi3* have been reported to be upstream of *Fgf8* (Vitelli et al., 2002b; Edlund et al., 2014; Hasten and Morrow, 2019). In $Foxi3^{-/-}$ embryos, *Fgf8* expression is greatly reduced in the ectoderm and endoderm, pc1 and pp1 do not form, and PA1 and PA2 fail to separate (Edlund et al., 2014). Interestingly, tissue-specific deletion of *Fgf8* in pp1 does not affect its morphogenesis or craniofacial development (Jackson et al., 2014; Jandzik et al., 2014). Extensive evidence supports a critical role for *Fgf8* expression, particularly from the oral ectoderm, in inducing PA1 mesenchymal gene expression regulating jaw patterning (e.g., Tucker et al., 1998; Trumpp et al., 1999; Ferguson et al., 2000; Fish et al., 2011; Griffin et al., 2013). The role of *Fgf8* expression in epithelial patterning and morphogenesis in mammals is less understood. We therefore examined pharyngeal epithelial morphogenesis, focusing on pp1 and pc1, in mouse embryos of varying *Fgf8* dosage.

The pharyngeal pouches develop serially from the primitive gut tube along the rostral-caudal axis (Veitch et al., 1999; Graham et al., 2005). Pouch morphogenesis relies on two separate morphogenetic processes, lateral out-pocketing and proximal-distal extension (Graham and Smith, 2001; Shone and Graham, 2014). Lateral out-pocketing is the process where the endoderm migrates laterally to contact the overlying ectoderm. Proximal-distal extension is the directional expansion of the pouch towards the midline of the embryo. Using an allelic series of *Fgf8* mice (Meyers et al., 1998), we characterized these processes in pp1 at varying *Fgf8* doses. Our data suggest that interaction between pp1 and pc1 may be required for proximal-distal extension of pp1 and separation of PA1 and PA2. Notably, in normal development, pp1 and pc1 establish a transient epithelial interface as they extend distally. This interface is disrupted in $Fgf8^{\Delta/Neo}$ embryos and the arches fail to separate. Our data highlights the importance of the first ectodermal cleft in jaw patterning and suggests it may be a target of alteration in both disease and evolution.

2 Methods

2.1 Experimental animals

The *Fgf8* allelic series utilizes 3 adult genotypes that can be crossed to generate five different embryonic genotypes (Meyers et al., 1998). Quantification of Fgf8 mRNA levels in E10.5 heads indicates that mice heterozygous for the Neo allele ($Fgf8^{Neo/+}$) express 90% of $Fgf8^{+/+}$ (wildtype; WT) levels, mice heterozygous for the Delta allele ($Fgf8^{\Delta/+}$) express 60% of WT levels, mice homozygous for the Neo allele ($Fgf8^{Neo/Neo}$) express 35% of WT levels, and compound mutants ($Fgf8^{\Delta/Neo}$) express 20% of WT levels (Green et al., 2017). These mice and embryos were genotyped as previously reported (Meyers et al., 1998; Green et al., 2017; Zbasnik et al., 2022). Embryos were collected and staged based on the number of days after the observation of a postcoital plug at E0.5. Mouse experiments were approved by the University of Massachusetts Lowell Institutional Animal Care and Use Committees. Embryos were dissected on ice and fixed in 4% paraformaldehyde.

2.2 *In situ* hybridization

Probes for *in situ* hybridization were generated from RNA isolated from E9.5 and E10.5 embryos. cDNA was produced using the Maxima

first strand synthesis kit (ThermoFisher; K1641). The cDNA was then used as a PCR template to amplify the gene of interest (GOI). Select PCR primers had linkers (Fw:5′-ggccgcgg-3'; Rv:5′ - cccggggc-3′) to allow for a nested PCR TOPO cloning. PCR purification of these templates used a gene specific forward primer (GSFP) and the T7 Universal primer to amplify the initial GOI template. Primers lacking linkers were TOPO cloned into TOP10 competent *E. coli* cells using a PCR4 topo vector (ThermoFisher). Colonies were screened to ensure correct band length. Once purified, samples were sequenced to ensure the correct GOI was amplified and direction of the insertion. A second PCR was used to amplify the GOI using M13 primers after plasmid verification. Second PCR product lengths were verified on a 1% agarose gel. Products from the secondary PCR were used as the template for the anti-sense mRNA probe. Probes were made by using a dig RNA labeling mix (Sigma-Aldrich; #11277073910). Fluorescent probes were created with A555 fluorescent tyraminein borate buffer (100 nM borate, 0.1% Tween, 0.003% H_2O_2). Fluorescent samples were counter-stained using Hoechst's O.N. (10 ug/mL) and were imaged using a 40x oil immersion objective lens on a Leica sp8 confocal microscope.

2.3 Immunofluorescence

Whole embryos were fixed in 4% PFA/PBS, permeabilized with 0.1% Triton-X-100/PBS and then blocked in 5% FBS supplemented with 0.1% BSA for 1 h. Primary antibodies used were: AP-2α (Santa Cruz sc-12726, 1:200 mouse), E-Cadherin (BD Transduction Laboratories 610181, 1:150 mouse), Laminin (Sigma-Aldrich L9393, 1:60 rabbit), and Sox2 (Millipore-Sigma AB5603-25UG, 1:1000 rabbit). The mitotic marker Phospho-Histone H3/Ser10 (Cell Signaling 9701, 1: 100 rabbit) was used to label proliferating cells. Secondary antibodies used against mouse were: Alexa488 (Abcam ab150113), Alexa647 (Invitrogen A-21240), Cy3 (Life Technologies A-10524) and against rabbit were: Alexa488 (Molecular Probes A11034), Alexa647 (Molecular Probes A21245). In conjunction with these antibodies, dyes were used to stain nuclei (Hoechst 1:1000), lysosomes to track cellular death (lysotracker Red) and F-actin cables (Phalloidin 1:1000). Embryos were imaged on a Nikon AR-1, a Leica Sp8, or a Zeiss Axiovert 200 M microscope. Images were processed using the Fiji distribution of ImageJ and Adobe Photoshop CC 2018.

2.4 Pouch shape analysis

Whole mount fluorescent *in situ* hybridization was performed for *Pax1*. Confocal images were collected at the point which the pouch opens and maintains contact with the cleft. Each side of the embryo was imaged through the total length of both the cleft and pouch until the first and second pouch connected. All left facing images were flipped along their vertical axis before landmarks were placed. 8 landmarks with 8 curves (semi landmark locations) were chosen to be digitized of each image for morphometric analyses. Stereomorph (version 1.6.3) a package within R (version 1.2.1335) was used to place these landmarks on each image. Once completed, the geomorphic package (version 3.3.2) was used to analyze the morphology of the first pouch.

A generalized procrustes analysis of the coordinates was performed using the gpagen function (Gower, 1975; Rohlf, 1990). The newly rotated and scaled shape data were then analyzed via procrustes ANOVA (procD.lm function). Additionally, a null model was made to verify if our chosen explanatory variables were contributing to shape changes. The null model was a fitted procrustes ANOVA of the shape coordinates with only the log transformed centroid size as a predictor variable. The full model ran against this null model included the log transformed centroid size, genotype, side, and somite number as predictor variables with all their interaction terms. An ANOVA was performed between the full and null model to verify if these two models were different. Finally, a principal component analysis (PCA) was performed on our coordinate data to generate a representative graph of pp1 shape change between *Fgf8* dosage levels. The gm.prcomp function was used to generate the graphs. Only younger (<23 somite pairs) and older (>28 somite pairs) embryos were used for the PCA analysis to maximize pp1 shape differences due to developmental age while ensuring we had enough samples in each group.

2.5 Quantification of out-pocketing depth

Imaging parameters were the same as the shape analysis, with a z-step set to 2.5um. We used 20X magnification (0.75 numerical aperture; 0.62 working distance). Each pouch was imaged from the point where the pp1 connects to pp2 medially through its full lateral extension. Depth was quantified by multiplying the number of frames by 2.5 µm. To test for significance, a general linear model was performed. Pouch depth was measured against the following fixed predictor variables: somite pairs (age), left or right side, and genotype. Somite pairs and genotype were treated as co-variates to take into consideration the effect *Fgf8* dosage has on embryo size.

2.6 Identification of pp1 and pc1

Expeimental embryos were processed in whole-mount and then imaged in 3D using confocal microscopy. Each embryo was evaluated throughout the scan to see where pp1 and pc1 originate (laterlly and mediall, respectively) and was then followed through the embryo to the point of contact. In early experiments, *Pax1* expression was used to confirm endoderm identity. Generally the pouch is a single cell epithelial band and is easily distinguishable. We considered pc1 as the area where the surface ectoderm invaginates, and was distinguished from the endoderm by Ap2-alpha staining. In the mutants that lack epithelial specific staining (either E-cad or Ap2-alpha) we relied heavily on the morphology of the structure utilizing the z-stack and tracking the tissue.

2.7 Apoptosis quantification

Dead or dying cells were labeled using a lysotracker red dye (L7528, thermo Fisher Scientific). Labeling of tissues were followed per manufacture guidelines. Imaging and quantification of all samples was performed together to ensure a standardized intensity of light was used for imaging between samples and that counting was standardized. Only cells localized in the mesenchyme between or next to the junction site of pp1/pc1 were quantified in the regions where pp1 first started to open

until pc1 fully closed. A student's t-test was performed to verify if the means between groups were different.

2.8 Specimens analyzed

Sample size of evaluated specimens based on experiment are described in Table 1.

TABLE 1 Description of samples used in experiments described in this study.

Experiment	Non-Mutant	Mutant	Age
Sox2	27	13	E9.5-10.5
Ap2-alpha	17	11	E9.5-10.5
Pax1 *in-situ*	15	10	E9.5-10.5
E-cadherin	12	5	E9.5-10.5
F-actin	13	5	E9.5-10.5
Laminin	12	5	E9.5-10.5
Fgf8 in-situ	9	7	E9.5
Depth Analysis	34	16	E8-10.5
Shape Analysis	34	16	E8-10.5
Proliferation (PH3)	5	4	E10.5
Cell Death (Lysotracker)	5	7	E10.5

3 Results

3.1 *Fgf8* reduction alters expression domains and epithelial shape

The *Fgf8* allelic series of mice consists of five genotypes that express *Fgf8* at different levels during development (Meyers et al., 1998). Mice heterozygous for the Neo allele ($Fgf8^{Neo/+}$) express 90% of $Fgf8^{+/+}$ (wildtype; WT) levels, mice heterozygous for the Delta/null allele ($Fgf8^{\Delta/+}$) express 60% of WT levels, mice homozygous for the Neo allele ($Fgf8^{Neo/Neo}$) express 35% of WT levels, and compound mutants ($Fgf8^{\Delta/Neo}$) express 20% of WT levels (Green et al., 2017). To further understand how dosage reductions impact *Fgf8* expression, we performed whole mount *in situ* hybridization in E8.5 embryos. In WT ($Fgf8^{+/+}$) embryos, *Fgf8* is strongly expressed throughout the endoderm (pp1, pp2) and in the splanchnic mesoderm, whereas in the ectoderm, expression is higher on the anterior side of pc1 (Figures 1A–C; see also Supplementary Figure S3M; Supplementary Movie S1). In $Fgf8^{\Delta/Neo}$ embryos, expression is not only reduced, but often mis-expressed. In the ectoderm, *Fgf8* extends into the proximal region where it is not normally expressed and is lost in the anterior region (red asterisk in pc1 Figures 1D, E). *Fgf8* expression is always reduced in the mutants, however mis-expression in the cleft is variable and seems to relate to variation in severity of defects in cleft morphogenesis. We observe that the first and second cleft are often connected (See Supplementary Figure S3O). *Fgf8* expression is greatly reduced in the endoderm and splanchnic mesoderm, which is typical for all $Fgf8^{\Delta/Neo}$ embryos we examined (Figures 1D–F; see also Supplementary Figure S3N; Supplementary Movie S2).

3.2 Out-pocketing of pp1 is largely robust to reductions in *Fgf8*

To further understand how reductions in *Fgf8* expression impact pharyngeal epithelial development, we first investigated pp1 morphogenesis. Pouch morphogenesis occurs via two separate morphogenetic processes, lateral out-pocketing and proximal-distal extension (Graham and Smith, 2001; Shone and Graham, 2014). Out-pocketing is the process where the

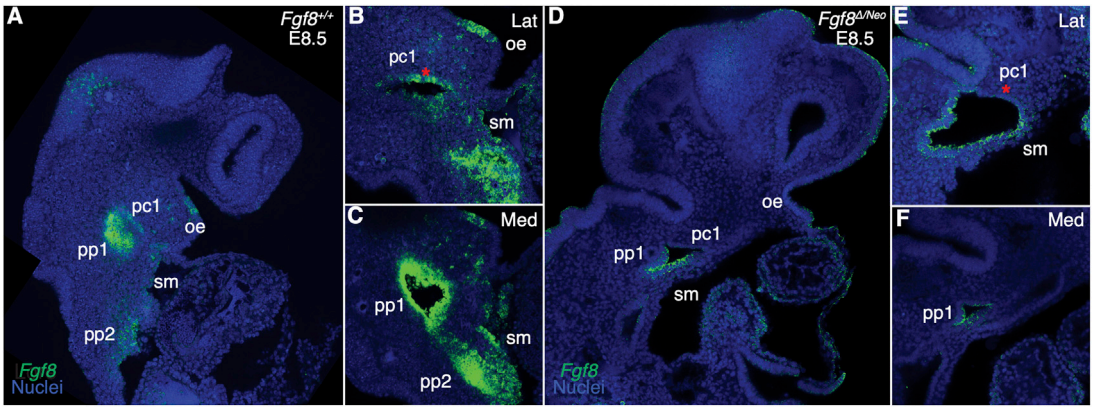

FIGURE 1
Fgf8 is reduced and mis-expressed in $Fgf8^{\Delta/Neo}$ epithelia. Confocal sections of whole-mount *in situ* hybridization for *Fgf8* In E8.5 embryos are shown for $Fgf8^{+/+}$ (WT; **(A–C)** and $Fgf8^{\Delta/Neo}$ **(D–F)** embryos. Expression is shown for an overview of the head **(A, D)** and higher magnification at a more lateral (Lat; **(B, E)** and more medial (Med; **(C, F)** sections. **(A–C)** At E8.5, *Fgf8* is typically expressed in the oral ectoderm (oe), the ectodermal clefts (pc1), endodermal pouches (pp1, pp2), and splanchnic mesoderm (sm). **(D–F)** In $Fgf8^{\Delta/Neo}$ embryos, *Fgf8* is overall reduced in the cleft and expressed in the ventral region of pc1, but absent in the anterior region [compare red asterisk in **(E, B)**]. Expression in the endoderm and splanchnic mesoderm is also greatly reduced **(F)**. Note that pc1 opens widely at the lateral surface of the embryo **(E)** which often results in pc1 and pc2 being continuous in $Fgf8^{\Delta/Neo}$ embryos. Images are representative of 9 (WT) and 7 ($Fgf8^{\Delta/Neo}$) embryos.

developing pouch extends along a lateral axis from the midline to contact the overlying ectoderm (Figure 2A). To determine how *Fgf8* dosage impacts pp1 lateral out-pocketing, we performed whole mount *in situ* hybridization for *Pax1* on E9.5 embryos and created 3D-reconstructions of pp1 from confocal images (Figure 2B). We chose E9.5 since pp1 and pc1 are in contact and out-pocketing is nearly complete at this stage. Out-pocketing was measured as the distance from the point where pp1 first opens from the foregut medially (Figure 2B, represented in, dark blue) to the lateral edge where it contacts pc1 (Figure 2B, represented in red). Absolute depth is similar in all genotypes except for $Fgf8^{\Delta/Neo}$, which have shallower pouches (Figure 2C; p <0.0001). However, lateral out-growth does occur in $Fgf8^{\Delta/Neo}$ embryos, and importantly, pp1 does contact pc1.

3.3 *Fgf8* is required for proximal-distal extension of pp1

To determine the effect of *Fgf8* dosage on proximal-distal extension, we quantified pp1 shape at the point where it contacts pc1 laterally for both early (12–23 somites) and late (28–31 somites) morphogenetic stages (Figure 3). In the initial stages of out-pocketing, pp1 grows laterally as a circular tube and is circular in shape when it contacts pc1. After contact, the distal edge of pp1 extends ventrally towards the midline, resulting in a triangular shaped pouch (Figures 3B, C upper panels). In $Fgf8^{\Delta/Neo}$ mutants, the pouch does not extend after out-pocketing, and instead remains circular (Figures 3B, C lower panels; see also Supplementary Figure S1). We calculated morphological disparity in pp1 shape between WT and each of the other 4 genotypes in the allelic series. Only $Fgf8^{\Delta/Neo}$ mutants have a statistically significant difference in shape from WT at late stages ($p < 0.001$). We did observe, however, subtle differences in the interior shape of pp1 in $Fgf8^{Neo/Neo}$ mutants at E10.5, but these are not significantly different from WT (Supplementary Figure S2). To further visualize these shape changes, we performed a Principal Component Analysis on the early- and late-stage WT and $Fgf8^{\Delta/Neo}$ pouch shapes (Figure 3D). Early-stage pp1 shapes occupy overlapping morphospace, which is also shared with late-stage $Fgf8^{\Delta/Neo}$ pouches. Late-stage WT pouches differ in shape, which is observed as a shift along PC1 (representing 40% of the variation; $p = 0.0178$). To visualize shape change, pp1 shapes at the extremes of each axis were compared (Figure 3E). The arrows show the direction of shape change associated with each permanent/semi landmark (black dots) between the two extremes. Along PC1, a majority of landmarks are associated with distal extension of pp1. A portion of the distal landmarks, those that are typically associated with and connected to pc1, are shown to be the main drivers in distal extension of pp1 (reflected in the length of the arrows). Further, the data indicates that as pp1 extends distally, it also compresses along the anterior-

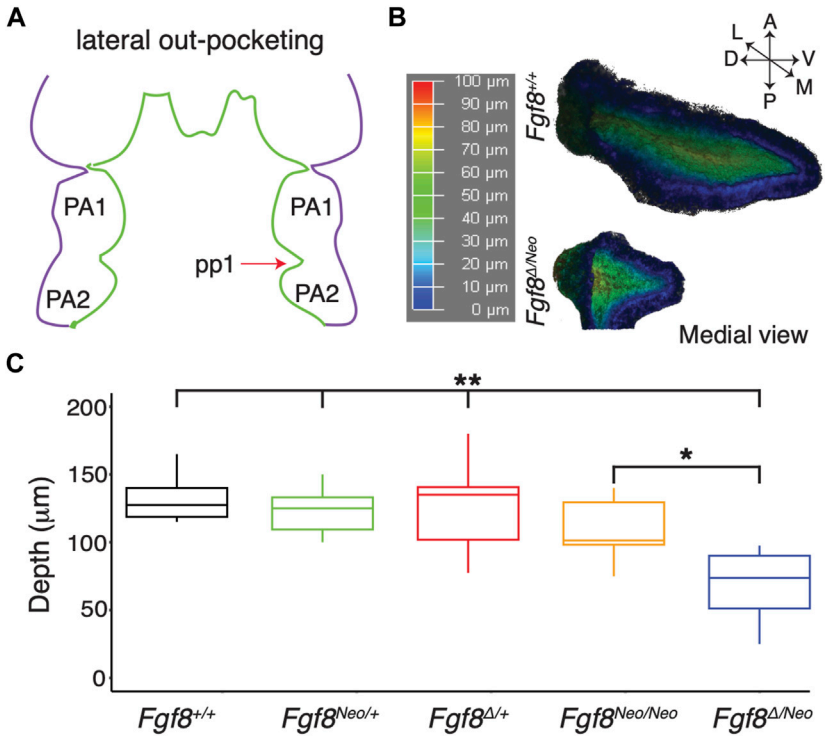

FIGURE 2
Lateral outgrowth of pp1 is robust to reductions in *Fgf8*. **(A)** The first stage of pharyngeal pouch (pp1) morphogenesis is lateral outgrowth to contact the overlying ectoderm between the first (PA1) and second (PA2) pharyngeal arches. **(B)** 3D reconstructions of pp1 were generated from confocal images of *Pax1* expression in the endoderm of E9.5 embryos. Dark blue colors represent tissue closer to the endoderm and dark red colors represent tissue closer to the ectoderm. **(C)** Only severe reductions of *Fgf8* typical of $Fgf8^{\Delta/Neo}$ embryos result in shallower pouches (p-values <0.0001 for all genotypes compared to $Fgf8^{\Delta/Neo}$ except $Fgf8^{Neo/Neo}$ where p <0.01). Images are representative of 34 (WT) and 16 ($Fgf8^{\Delta/Neo}$) embryos.

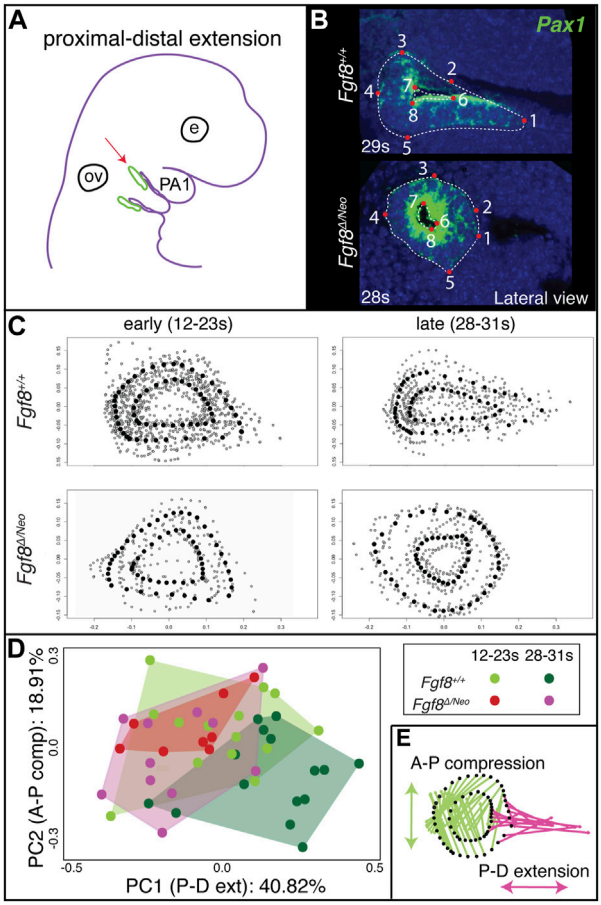

FIGURE 3
Proximal-distal extension fails in *Fgf8*$^{\Delta/Neo}$ pouches. **(A)** After out-pocketing, pp1 extends distally towards the jaw midline (red arrow points to pp1 in green). **(B)** A landmark-based analysis was used to measure the shape and distal extension of pp1 in *Fgf8*$^{+/+}$ (WT shown at 29 somites (s); upper panels) and *Fgf8*$^{\Delta/Neo}$ (shown at 28 somites (s); lower panels) embryos. Eight permanent (red dots) and semi landmarks (white dashed lines) were placed on each image. **(C)** Shape analysis was conducted on early (12–23 s; left) and late stage (28–31 s; right) embryos. **(D)** A Principal Component analysis was conducted over the shape of the pouches of early (12–23 s) and late stage (28–31 s) *Fgf8*$^{+/+}$ (green) *Fgf8*$^{\Delta/Neo}$ (pink) embryos. **(E)** Shape change represented by PC1 is shown. The pink arrows represent distal extension. Green arrows reflect anterior-posterior compression. See text for more discussion. Images are representative of 34 (WT) and 16 (*Fgf8*$^{\Delta/Neo}$) embryos. E, eye; ov, otic vesicle.

posterior axis. These data suggest that *Fgf8* is required for both distal extension and anterio-posterior compression of pp1.

3.4 Staging of pharyngeal epithelial morphogenesis

To further understand how *Fgf8* reductions alter pp1 morphogenesis, we generated a standard developmental scheme for WT embryos documenting tissue interactions between pp1 and pc1 (Figure 4; Supplementary Figure S3). We defined 4 stages corresponding to E8.5 (pouch initiation), E9.0 (contact), E9.5 (pharyngeal plate formation), and E10.5 (pharyngeal plate modification). At E8.5 (Pouch Initiation), pp1 initiates out-pocketing. The foregut endoderm of pp1 extends laterally as a circular epithelial sheet towards the ectoderm (pc1). The lateral growth of pp1 occurs posterior to pc1. During the initiation stage, pp1 and pc1 are separate epithelial sheets that do not come into contact (Figures 4A, E–G). At E9.0 (Contact), the lateral growth of pp1 results in contact with pc1 (Figure 4I). At this stage, the pouch is still mostly circular in shape at the point of contact, but is more open and extended medially where it is not in contact with pc1 (Figures 4I, J). Notably, the entire anterior side of pp1 is in contact with pc1 at its posterior-proximal edge (Figure 4I). At E9.5 (Pharyngeal Plate Formation), lateral extension of pp1 continues along the proximal region of pc1 (Figures 4L, M). At this stage, continuous contact between pp1 and pc1 occurs with the anterior side of pp1 contacting the posterior-proximal aspect of pc1. Invagination of pc1 and outgrowth of pp1 result in more overlap along the medial-lateral axis. Also at this stage, pc1 is closing at both its proximal and distal ends as the anterior and posterior ectodermal layers come in contact, a process we refer to as "zippering" (Figure 4L). At E10.5 (Plate Modification), the relationship of pp1 and pc1 has changed such that the lateral aspect of pp1 is now proximal to pc1, which continues to close distally. Despite these changes, the proximal edge of pp1 remains in contact with pc1 (Figures 4N–P).

3.5 Cleft morphogenesis is abnormal in *Fgf8*$^{\Delta/Neo}$ embryos

Since *Fgf8*$^{\Delta/Neo}$ embryos showed significant defects in pp1 morphogenesis, we characterized pharyngeal epithelial development in *Fgf8*$^{\Delta/Neo}$ embryos at the 4 stages of development described for WT (Figure 4; Supplementary Figure S3). *Fgf8*$^{\Delta/Neo}$ embryos exhibit highly variable defects, but some overall trends can be noted. From the earliest stage (pouch initiation) pc1 is larger and more open in *Fgf8*$^{\Delta/Neo}$ embryos compared to WT (Figures 4A′, E′). Contact between pp1 and pc1 often occurs earlier (already in the initiation phase) than in WT (Figures 4F′, G′), which may be related to the smaller overall size of these embryos (early contact was observed in 2/7 embryos). However, this early contact does not occur in all embryos, and can even be delayed into the pharyngeal plate formation stage (Figures 4H′–J′, K′–M′). In all cases, when contact between pp1 and pc1 occurs, it is limited temporally and spatially. Further, the position of pp1 relative to pc1 is often abnormal in the mutants. In WT, pp1 contacts pc1 at its proximal-posterior edge (Figure 4I). However, in *Fgf8*$^{\Delta/Neo}$ embryos, pp1 contact with pc1 is highly variable and can been seen anterior to pc1 or very distal along pc1 (Figures 4L′, O′). Notably, during the pharyngeal plate formation stage, pp1 in *Fgf8*$^{\Delta/Neo}$ embryos does not align such that its anterior side is in contact with pc1. Rather, the proximal-anterior side of pp1 is often separated from pc1 by mesenchymal cells (Figures 4O′, P′; see also Figure 5D).

Finally, as noted above, a normal part of pc1 morphogenesis is the process of closing, or zippering, the cleft. In WT embryos, this zippering can begin as early as E9.0 (contact) and is ongoing through E10.5 (plate modification). In *Fgf8*$^{\Delta/Neo}$ embryos, this zippering process is incomplete, and in many cases, pc1 remains open and contacts pc2 creating a large lateral opening (Figures 4K′, N′, O′; Supplementary Figure S3O). Overall, the mutants exhibit significant variability in defects.

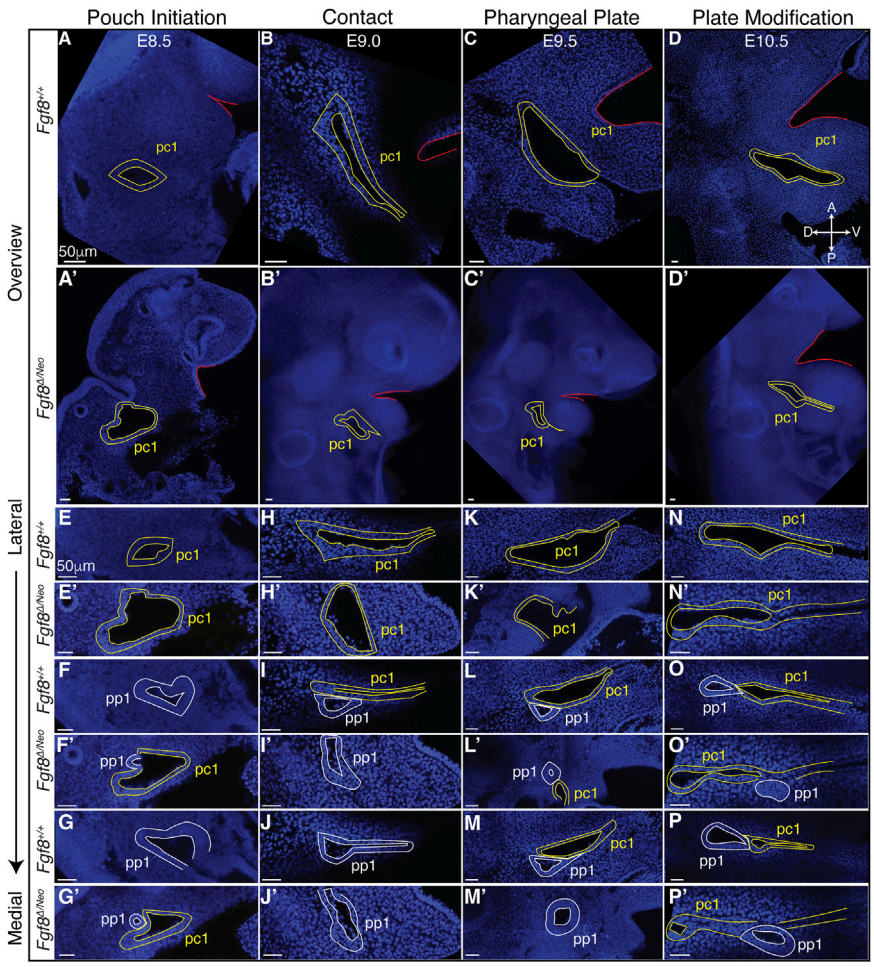

FIGURE 4
Staging of pharyngeal epithelial morphogenesis in WT and in *Fgf8*$^{\Delta/Neo}$ embryos. Confocal sections from whole-mount *Fgf8*$^{+/+}$ [WT; **(A–P)**] and *Fgf8*$^{\Delta/Neo}$ embryos **(A′–P′)** are shown providing an overview of the first cleft (pc1; yellow outline) of each developmental stage at a point before the first pouch (pp1; white outline) opens in relation to the oral ectoderm (red outline) **(A–D, A′–D′)** and at higher magnification for three different sagittal sections from lateral to medial **(E–P, E′–P′)**. The panels are orientated with anterior side up and ventral (distal) on the right. Each column depicts the relationship between pp1 and pc1 at 4 different morphogenetic phases: Pouch initiation, Contact, Pharyngeal Plate Formation, and Pharyngeal Plate modification. Orientation of the embryos in anterior (A), posterior (P), dorsal (D), and ventral (V) is shown in panel **(D)** and applies to all panels. See text for more details.

Nonetheless, in all cases, pp1and pc1 fail to completely extend, and therefore, PA1 and PA2 do not segment distally (Figure 4D′).

3.6 Epithelial molecular identity is altered in *Fgf8*$^{\Delta/Neo}$ mutants

To better characterize *Fgf8*-mediated defects in epithelial morphogenesis, we investigated cellular identity in pp1 and pc1 during pouch extension (E9.5-10.5). We performed immunostaining with Sox2, which is expressed in the foregut endoderm (Que et al., 2007), and AP2-alpha, which is expressed in the facial surface ectoderm (Van Otterloo et al., 2022). In WT, we observe that Sox2 is expressed throughout pp1 at the medial side (towards the foregut; Supplementary Figures S4A, G′), however, more laterally where pp1 and pc1 are in contact, Sox2 is only expressed in cells in the distal portion of pp1 where extension is occurring and where pp1 maintains contact with pc1 (Figures 5A, B; Supplementary Figures S4A, E′). Notably, the proximal-posterior region of pc1 that is in contact with the distally extending endoderm is also positive for Sox2, forming a continuous region of Sox2 expression across the pp1/pc1 border (Figure 5B). The Sox2 positive cells in the ectoderm (pc1) are also AP2-alpha positive. In contrast, Sox2 labeling is severely reduced in E9.5 *Fgf8*$^{\Delta/Neo}$ pouches and completely absent in pp1 by E10.5 (Figures 5C, D). Sox2 is also not expressed in pc1 and the region of co-expressing Sox2/AP2-alpha cells is absent (Supplementary Figures S4B, H′–J′).

3.7 *Fgf8* mediates downregulation of E-cadherin in pc1

Since cadherins have previously been identified as mediators of pouch morphogenesis (Quinlan et al., 2004), we evaluated E-cadherin localization in WT and *Fgf8*$^{\Delta/Neo}$ embryos. In both

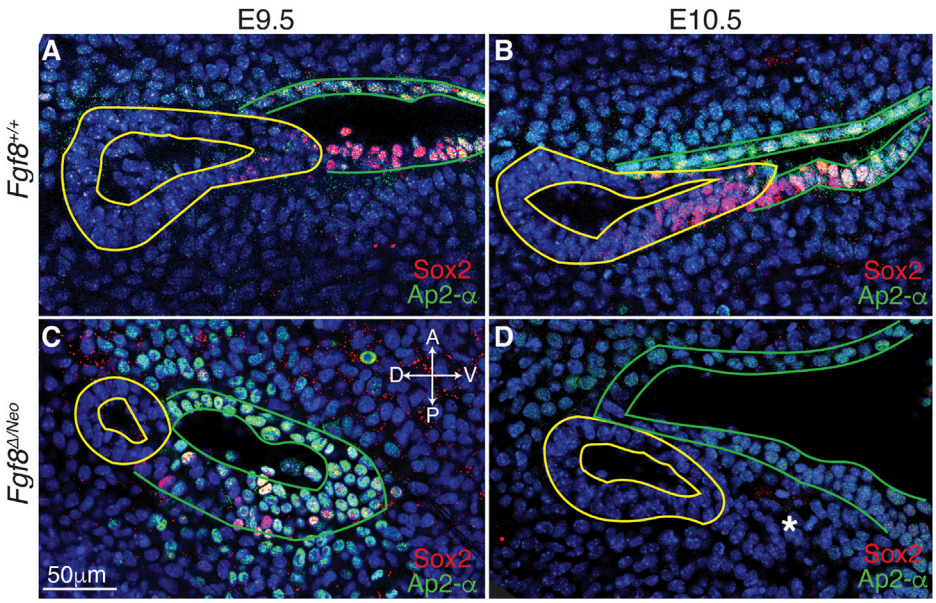

FIGURE 5
Cellular identity is altered in pp1 and pc1 of *Fgf8* $^{\Delta/Neo}$ embryos. Confocal sections of immunostaining for Sox2 (red) and Ap2-alpha (green) in pp1 (yellow outlines) and pc1 (green outlines) of *Fgf8*$^{+/+}$ (WT; **(A, B)** and *Fgf8*$^{\Delta/Neo}$ **(C, D)** at E9.5 **(A, C)** and E10.5 **(B, D)** are shown. In *Fgf8*$^{+/+}$ (WT), all cells in pc1 are Ap2-a positive at both E9.5 and 10.5 **(A, B)**. Additionally, Sox2 positive cells occupy the posterior-distal extending edge of pp1 and the posterior-proximal region of pc1. In *Fgf8*$^{\Delta/Neo}$ embryos, pp1 lacks Sox2 expression entirely, and Ap2-a expression is much lower in pc1. In E10.5 *Fgf8*$^{\Delta/Neo}$ embryos, the posterior-distal extending edge of pp1 and the posterior-proximal region of pc1 are not connected. The panels are orientated with anterior side up and ventral (distal) on the right. The white asterisk in **(D)** indicates a group of cells that appear to "bleb" from pp1 in this particular confocal plane. Orientation of the embryos in anterior (A), posterior (P), dorsal (D), and ventral (V) is shown in panel **(C)** and applies to all panels. n > 10 for each staining (see Table 1).

WT and *Fgf8*$^{\Delta/Neo}$ E9.5 embryos, E-cadherin is expressed uniformly throughout pp1 and pc1 (Figures 6A, B). However, in WT by E10.5, E-cadherin is heterogeneous in pc1 due to localized reduction in the proximal-posterior ectoderm (Figures 6D, I, J; Supplementary Figures S4C, G′). This area of reduced E-cadherin expression corresponds to the Sox2/AP2-alpha double-positive region described above (Figure 6I). In contrast, at E10.5 in *Fgf8*$^{\Delta/Neo}$, E-cadherin levels remain high in both the anterior and posterior layers that interface with pp1 (Figures 6F, K, L; Supplementary Figure S4D). Additionally, in WT embryos the cleft is relatively deep with a sharp slope of cells expressing E-cadherin stacked along the medio-lateral axis (Figures 6C, E), whereas pc1 is shallow in *Fgf8*$^{\Delta/Neo}$ embryos (Figures 6G, H). Taken together, our data suggest that E-cadherin expression is normally downregulated in the posterior-proximal region of pc1 that interfaces with pp1 (a region that is also Sox2 positive), and that this downregulation does not occur in *Fgf8*$^{\Delta/Neo}$ embryos.

3.8 Cell polarity is altered at the epithelial interface

Previous work has described that disruption to actin cables results in failure of pouch extension in chick embryos (Quinlan et al., 2004). To test if failure of pp1 extension in *Fgf8*$^{\Delta/Neo}$ embryos was associated with disruption to actin cables, we used phalloidin to label F-actin (Supplementary Figure S5). In E9.5 WT pp1, F-actin is localized at the apical side of cells within pp1 (Supplementary Figure S5A). However, in the anterior-distal region where it contacts pc1, F-actin is more equally distributed around the cell and is also located basally (Supplementary Figure S5B; yellow arrow). In E9.5 *Fgf8*$^{\Delta/Neo}$ pp1, F-actin is highly localized on the apical side of pc1 and pp1, but no basal localization is present at the site of contact (Supplementary Figure S5F; yellow arrow). To further assess cell polarity, we examined laminin localization. In *Fgf8*$^{+/+}$ (WT), laminin exhibits a strong basal localization in cells on the anterior side of pc1 and in cells at the proximal and anterior edges of pp1 (Supplementary Figures S5C, D). However, in the region where pp1 and pc1 are in contact, laminin is highly expressed, but lacks basal polarization (Supplementary Figure SC; white arrow). In *Fgf8*$^{\Delta/Neo}$ embryos, laminin is reduced, but remains polarized (Supplementary Figures S5G, H; white arrow in G). These data suggest that some alterations to cell polarity including the actin cytoskeletal network normally occurs in both pp1 and pc1 near the site of contact between these epithelia. We observed subtle differences in laminin and F-actin in *Fgf8*$^{\Delta/Neo}$ embryos relative to WT which may contribute to the observed disruptions in epithelial interactions at the interface.

3.9 *Fgf8* mediates mesenchymal cell death at the endodermal-ectodermal interface

Finally, since *Fgf8* is known to regulate cell survival and proliferation (Trumpp et al., 1999; Compagnucci et al., 2021), we

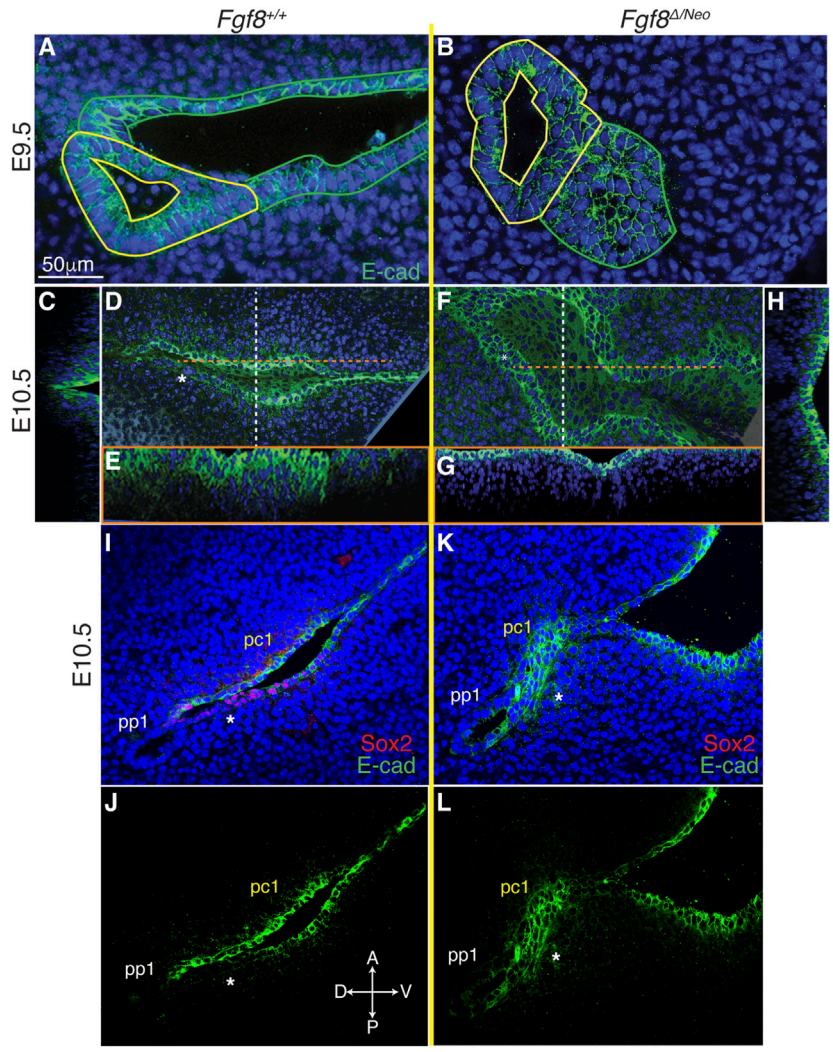

FIGURE 6
Fgf8 mediates downregulation of E-cadherin in pc1 at the pharyngeal plate. Confocal images of E-cadherin immunostaining (green) in pp1 (yellow outlines) and pc1 (green outlines) of $Fgf8^{+/+}$ (WT; **(A, C–E)** and $Fgf8^{\Delta/Neo}$ **(B, F–H)** at E9.5 **(A, B)** and E10.5 **(C–H)** are shown. At E9.5, E-cadherin is expressed throughout pp1 and pc1 in both $Fgf8^{+/+}$ (WT; **(A)** and $Fgf8^{\Delta/Neo}$ **(B)** embryos. **(D–H)** Lateral and cross-section views of E10.5 embryos. Cross sections are color coded as dashed lines in the lateral views **(D, F)** as vertical (white; **(C, H)** or horizontal (orange; **(E, G)**. The overview panels are orientated with anterior on top and distal to the right. **(D)** By E10.5 in $Fgf8^{+/+}$ (WT), E-cadherin is downregulated in pc1 in the proximal-posterior region (white asterisk) that connects with pp1 at the pharyngeal plate. **(C, E)** At this stage, the cleft is closing along the proximal-distal axis, forming a deep, narrow groove. **(F)** In contrast, E-cadherin remains upregulated and relatively homogenous in pc1 of E10.5 $Fgf8^{\Delta/Neo}$ embryos. **(G, H)** The cleft remains open, forming a wide, shallow groove. **(I–L)** Confocal images of E-cadherin (green) and Sox2 (red) immunostaining in pp1 and pc1 of $Fgf8^{+/+}$ (WT; **(I, J)** and $Fgf8^{\Delta/Neo}$ **(K, L)** at E10.5. Asterisk lies under the posterior epithelial layer of pc1. Note that relative to the anterior side in WT **(J)**, E-cadherin is downregulated in the posterior layer. This region of E-cadherin downregulation is Sox2 positive **(I)**. In $Fgf8^{\Delta/Neo}$ **(K, L)** E-cadherin is equally expressed in both layers of pc1 and Sox2 expression is negligible **(K)**. n > 5 for each staining (see Table 1).

evaluated cell death and proliferation in E10.5 pharyngeal epithelia. We found very few pH3 positive cells in pp1 of WT or $Fgf8^{\Delta/Neo}$ embryos (data not shown). In contrast, cell death (monitored by lysotracker staining) was prevalent in both the epithelia and in the mesenchyme surrounding the epithelial interface (Figures 7A–D). In WT there are numerous dying cells in the proximal epithelial region of pc1, the distal epithelial region of pp1, and in the mesenchyme between pp1 and pc1 at the region of contact (Figures 7A, C). Notably, $Fgf8^{\Delta/Neo}$ embryos exhibit almost no cell death in the interface region (Figures 7B, D). These data suggest that mesenchymal cell death is an important component of pp1 and pc1 interaction that is lost in $Fgf8^{\Delta/Neo}$ embryos (Figure 7E).

4 Discussion

4.1 *Fgf8* regulates pharyngeal epithelial development

Segmentation of the pharyngeal arches is required for patterning and differentiation of the oro-pharyngeal skeleton. The formation of

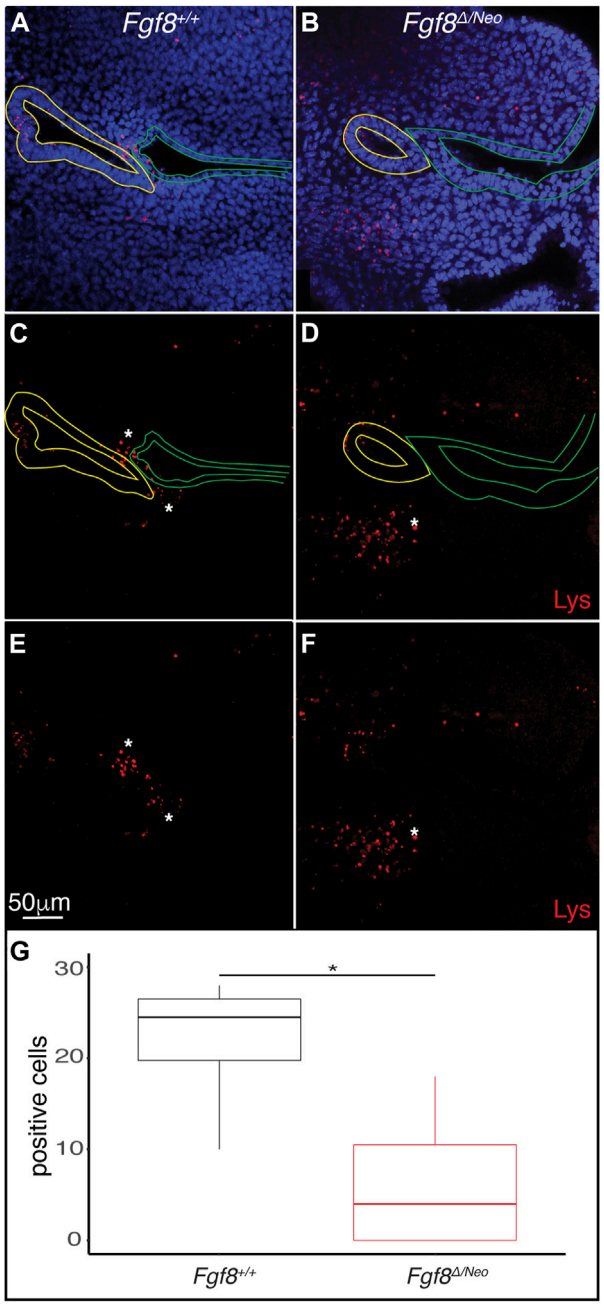

FIGURE 7
Fgf8 induces cell death in the mesenchyme surrounding the pharyngeal plate. Confocal sections of lysotracker staining (red) in pp1 (yellow outlines) and pc1 (green outlines) of $Fgf8^{+/+}$ (WT; **(A, C, E)** and $Fgf8^{\Delta/Neo}$ **(B, D, F)** at E10.5 are shown. Many lysotracker positive cells occupy pp1 of $Fgf8^{+/+}$, but not $Fgf8^{\Delta/Neo}$. Additionally, many mesenchymal cells surrounding the location where pp1 and pc1 are connected in $Fgf8^{+/+}$, but not $Fgf8^{\Delta/Neo}$, embryos. Panels **(E, F)** are the same as **(C, E)**, respectively, but shown without epithelial outlines. **(G)** Quantification of lysotracker positive cells in the mesenchyme near the pouch-cleft connection. Student T-test; *p*-value = 0.0126. n > 5 for each staining (see Table 1).

ectodermal–endodermal interfaces is a key mediator of this process (Graham, 2001, 2003; Couly et al., 2002; Crump et al., 2004; Edlund et al., 2014). Although this process is essential, mechanisms regulating endodermal out-pocketing and the establishment of epithelial interfaces vary between between vertebrate taxa and along the anterior-posterior axis within species. For example, in mice, endodermal out-pocketing involves epithelial bending, whereas in zebrafish, the pharyngeal pouches out-pocket through de-epithelialization and subsequent reconstruction of the epithelial sheet (Choe et al., 2013; Tsuchiya et al., 2018). Additionally, differences in ectodermal–endodermal interfaces between pp1 and the more posterior pouches have been described for mouse, chick, zebrafish, and shark (Shone and Graham, 2014). Here, we specifically focus on morphogenesis of pp1, in context with pc1, and the role of *Fgf8* dosage in this process in mouse embryos. We find that severe reductions of *Fgf8* levels ($Fgf8^{\Delta/Neo}$) disrupt both pp1 and pc1 development. Initially, pp1 does out-pocket and grow laterally to contact the ectoderm, although the total depth of pp1 is reduced compared to the other genotypes (Figure 2). Reduction in depth may result, in part, due to reduction in size of the embryo, however, even though pp1 contacts the ectoderm, the topological relationship of pp1 to pc1 at the initial point of contact is often abnormal. Subsequently, interactions between pp1 and pc1 are altered and extension of both pp1 and pc1 is incomplete (Figure 3). As a consequence, the first and second arches fail to separate distally.

To further understand mechanisms underlying these defects, we generated a staging series of epithelial morphogenesis in WT embryos (Figures 4, 8). Out-pocketing of pp1 begins as a circular tube. When pp1 contacts pc1 laterally, the entire anterior side of pp1 aligns with the proximal-posterior portion of pc1. We refer to this region of contact as the pharyngeal plate (see discussion below). After contact, pp1 and pc1 extend distally together. During this process, pc1 is also elongating and "zippering" closed at both ends. Together, the connection and extension of pp1 and pc1 create a long epithelial barrier that segments PA1 and PA2 (Figure 8). Importantly, the distal-anterior aspect of pp1 remains connected to pc1 throughout the extension process. Contact between pp1 and pc1 is mediated by reduction of E-cadherin, which occurs in a region of pc1 that is both Sox2 and AP2-alpha positive (Figures 5, 6, 8). Further, a continuous sheet of endodermal and ectodermal cells share Sox2-positive identity across the region of contact between pc1 and pp1 (Figures 5A, B).

In $Fgf8^{\Delta/Neo}$ embryos, these processes differ in several key aspects (Figures 4, 8). First, the initial contact between pp1 and pc1 is highly variable and typically abnormal. Instead of forming an extended region of overlap between the epithelial layers, the proximal end of pp1 is separated from pc1 by mesenchymal cells. E-cadherin remains high in the posterior side of pc1 and Sox2 expression is absent in both pp1 and pc1 of $Fgf8^{\Delta/Neo}$ embryos (Figures 5C, D, 6). Notably, pp1 fails to extend and instead remains circular in shape. Additionally, pc1 remains open rather than zippering closed. As neither pp1 or pc1 fully extend, PA1 and PA2 fail to segment distally.

4.2 Tissue-specific roles for *Fgf8*

Previous work involving tissue-specific loss of *Fgf8* has shown that *Fgf8* is not required in the endoderm for pp1 morphogenesis or arch segmentation in mice (Jackson et al., 2014). Loss of *Fgf8* in the ectoderm using either a nestin-Cre or AP2-alpha-Cre, results in very severe phenotypes with almost complete loss of the jaw

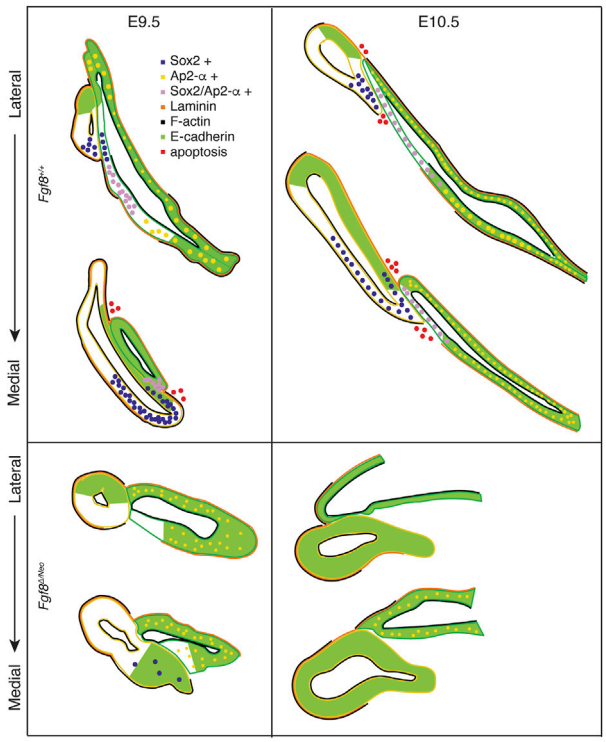

FIGURE 8
Fgf8 regulates pharyngeal epithelial tissue interactions. Model summarizing tissue interactions between pp1 (yellow outline) and pc1 (green outline) for both *Fgf8* $^{+/+}$ (WT) and *Fgf8*$^{\Delta/Neo}$ at E9.5 (early stage; left) and E10.5 (late stage; right) embryos. This model describes typical interactions and protein localization. For *Fgf8*$^{\Delta/Neo}$, in particular, both morphology and molecular outcomes are highly variable. See text for more details.

(Trumpp et al., 1999; Macatee et al., 2003). These phenotypes are more severe than those of the *Fgf8*$^{\Delta/Neo}$ mutants, and in the case of *Fgf8;Nestin-Cre* embryos, were shown to be correlated with massive apoptosis in PA1 (Trumpp et al., 1999). Because some expression in the lateral ectoderm remains in *Fgf8;Nestin-Cre* embryos, it was interpreted that loss of *Fgf8* in the oral ectoderm drove this extreme phenotype (Trumpp et al., 1999). Notably, apoptosis in post-migratory NC within PA1 is not observed in *Fgf8*$^{\Delta/Neo}$ embryos (Zbasnik et al., 2022). Mesoderm specific loss of *Fgf8* has been investigated through mesoderm (Mesp1-Cre) specific knock-out of *Tbx1* (which is upstream of *Fgf8*), as well as *Fgf8* specific deletion using Mesp1-Cre and Isl1-Cre (Park et al., 2006; Zhang et al., 2006). The focus of these mesodermal knock-out experiments was to investigate outflow tract formation, and details of first arch epithelial morphogenesis were not reported. Nonetheless, defects in pouch morphogenesis are described, with pp1 being less affected than the posterior pouches, but no information on pc1 is reported (Park et al., 2006; Zhang et al., 2006). Additionally, in zebrafish, *Fgf8* expression in the mesoderm is required for pouch out-pocketing, however, impacts on cleft morphogenesis are not reported (Crump et al., 2004; Choe and Crump, 2014). In any case, our data indicate that pp1 out-pocketing is more robust to reductions in *Fgf8* than is proximal-distal extension, which fails for both pp1 and pc1 in *Fgf8*$^{\Delta/Neo}$ mutants.

Notably, the mandibular phenotype in *Tbx1*$^{-/-}$ embryos is much less severe than what is observed in *Fgf8*$^{\Delta/Neo}$, rather it resembles the mildest phenotypes observed in *Fgf8*$^{Neo/Neo}$ neonates where only the coronoid process is missing (Jerome and Papaioannou, 2001; Zbasnik et al., 2022). Since *Fgf8* expression in pp1 and the splanchnic mesoderm, but not pc1, is regulated by *Tbx1*, this suggests that ectodermal *Fgf8* expression is a key driver behind the *Fgf8*$^{\Delta/Neo}$ mandibular phenotype. Deciphering tissue-specific roles for *Fgf8*, especially separating its role in the oral *vs*. lateral ectoderm will require more investigation. Nonetheless, our data suggest that *Fgf8* expression in the lateral surface ectoderm of pc1 is essential for arch segmentation. Importantly, in mice, arch segmentation involves extension of both pp1 and pc1. *Fgf8* is required for pc1 invagination, elongation, and zippering closed (Figures 4, 6). *Fgf8* is also required to specify regional cell identity in both pp1 and pc1 to upregulate Sox2 and downregulate E-cadherin, mediating their interaction and extension.

We also observe that laminin is not polarized basally in the region where pp1 and pc1 overlap. Similar observations have been made for first pouch-cleft interface in other vertebrate taxa, which were interpreted as a breakdown of the basement membrane (Shone and Graham, 2014). Despite this observation, Shone and Graham (2014) argue that no mixing of tissues occurs, with the ectoderm and endoderm remaining separate. We also find no evidence for cell mixing, but rather hypothesize this mediates interaction between the tissues for distal extension. This interaction is transient, and these layers separate by E11.5 to continue their individual differentiation (Kitazawa et al., 2015). Overall, our data indicate a critical role for the lateral surface ectoderm in arch segmentation that has previously been under-appreciated. A better understanding of how *Fgf8* is differentially regulated in the pharyngeal tissues, both in terms of its expression and its targets (autocrine *vs*. paracrine) will be important to elucidate its potential impacts in disease, especially as a modifier and contributor to phenotypic variability of 22q11 deletion Syndrome.

4.3 Boundary formation and patterning in pharyngeal development

Segmentation of the arches can also be characterized as compartmentalization, allowing separate mesenchymal cell populations to have distinct gene expression patterns and ultimately form unique skeletal elements. Compartmentalization is a critical developmental process that establishes boundaries between cell populations and also typically involves the formation of a signaling center that directs patterning after cell segregation (Dahmann and Basler, 1999; Kindberg and Bush, 2019; Pujades, 2020). The integration of pc1 and pp1 and their co-extension creates a physical boundary separating mesenchymal populations and preventing future cell mixing. We hypothesize that this contact is also critical to the formation of a signaling center organizing PA1 patterning. We have previously shown that failure to segment PA1 and PA2 in *Fgf8*$^{\Delta/Neo}$ embryos is associated with alterations to the expression of patterning genes (Zbasnik et al., 2022). The region of contact between pp1 and pc1, referred to as the pharyngeal plate, occurs near the mid-point (intermediate region) of PA1, underlying the area that curves between the upper (maxillary) and lower (mandibular) portions of the arch.

The Hinge and Caps model of jaw development proposes that signaling interactions between the pharyngeal plate and the oral ectoderm generate a signaling center at the mid-point of PA1 (Depew and Simpson, 2006; Depew and Compagnucci, 2008). Several key lines of evidence support existence of a secondary organizer at the Hinge, or mid-point, of PA1. First, loss or gain of function experiments manipulating regulators of jaw identity (e.g., Dlx5/6, Edn1) result in skeletal transformations that occur as mirror-images (Gendron-Maguire et al., 1993; Rijli et al., 1993; Depew et al., 2002b; Sato et al., 2008). Manipulations involving organizers typically induce mirror-image duplications because the organizer establishes a reference point for positional information (Anderson and Stern, 2016). Second, exogenous *Shh* expression near the pharyngeal plate results in duplication of juxtaposed domains of *Shh*, *Fgf8*, and *Bmp4* in the PA1 epithelia. As a result of this duplication of signaling interactions, the lower jaw skeleton is duplicated (Brito et al., 2006). Similar results have been shown for endoderm (*Shh*-expressing tissue) transplants in the pharyngeal plate region (Couly et al., 2002).

Our data further support the Hinge and Caps model and indicate that malformations in jaw development in *Fgf8* mutant mice result, in part, from disruptions to the jaw organizer. For proper tissue development, a signaling center must not only generate sufficient signals, but also be precisely oriented to provide accurate positional information. Our data suggest that $Fgf8^{\Delta/Neo}$ embryos fail to form a pharyngeal plate-pp1 and pc1 have limited physical interaction and the shared molecular identity observed in WT embryos in this region is lost in mutant embryos. Therefore, appropriate signals may not be generated from these tissues. Further, severe reductions in *Fgf8* result in dysmorphic pp1 and pc1 epithelia that have altered orientations relative to the oral ectoderm. Thus, whatever signals do emenate from these epithelia will be mis-oriented.

4.4 Evolution of the pp1 morphogenesis and origins of the jaw

The origin of the jaw is associated with an enlargement and modification of PA1 relative to the posterior arches (Kuratani, 2012). Notably, it curves near its mid-point forming an upper, maxillary and lower, mandibular portion. Similarly, pp1 is the largest of the pouches and its morphogenesis follows PA1 curvature, resulting in a pouch, that is, oblique, rather than parallel to, the posterior pouches. Molecular differences also exist between pp1 and the posterior pouches, which have been observed across a broad range of taxa (Quinlan et al., 2002; Shigetani et al., 2002; Piotrowski et al., 2003; Crump et al., 2004; Okubo et al., 2011; Choe et al., 2013). These data suggest that some aspect of pp1 development may be associated with the evolution of the jaw, which may be related to signaling interactions between pp1 and pc1 at the pharyngeal plate. In this regard, it would be important to identify conserved elements in pharyngeal plate identity among jawed vertebrates. The extent and relationship of the interaction between pp1 and pc1 requires more in-depth analysis across a broader range of taxa to determine what fundamentally characterizes this signaling center. For example, the interaction between pp1 and pc1 has been reported to be brief in chick embryos, but a detailed characterization may reveal some conserved elements (Shone and Graham, 2014). Additionally, comparisons of PA1 epithelial relationships and identity in lamprey with those from a broad range of jawed vertebrates will be required to address these hypotheses.

Data availability statement

The original contributions presented in the study are included in the article/Supplementary Material, further inquiries can be directed to the corresponding author.

Ethics statement

The animal study was reviewed and approved by the University of Massachusetts Lowell IACUC.

Author contributions

NZ and JF contributed to the conception, design, and performance of the study. NZ and JF contributed to the writing and revision of the manuscript. All authors contributed to the article and approved the submitted version.

Funding

This work was supported by the National Institutes of Health: R03 DE028984 and R15 DE026611 to JF.

Acknowledgments

We would like to thank Evelyn Schwager for technical support.

Conflict of interest

The authors declare that the research was conducted in the absence of any commercial or financial relationships that could be construed as a potential conflict of interest.

Publisher's note

Supplementary material

The Supplementary Material for this article can be found online at: https://www.frontiersin.org/articles/10.3389/fcell.2023.1186526/full#supplementary-material

References

Anderson, C., and Stern, C. D. (2016). Organizers in development. *Curr. Top. Dev. Biol.* 117, 435–454. doi:10.1016/bs.ctdb.2015.11.023

Arnold, J. S., Werling, U., Braunstein, E. M., Liao, J., Nowotschin, S., Edelmann, W., et al. (2006). Inactivation of Tbx1 in the pharyngeal endoderm results in 22q11DS malformations. *Development* 133 (5), 977–987. doi:10.1242/dev.02264

Brito, J. M., Teillet, M. A., and Le Douarin, N. M. (2006). An early role for sonic hedgehog from foregut endoderm in jaw development: Ensuring neural crest cell survival. *Proc. Natl. Acad. Sci. U. S. A.* 103 (31), 11607–11612. doi:10.1073/pnas.0604751103

Choe, C. P., Collazo, A., Trinh le, A., Pan, L., Moens, C. B., and Crump, J. G. (2013). Wnt-dependent epithelial transitions drive pharyngeal pouch formation. *Dev. Cell* 24 (3), 296–309. doi:10.1016/j.devcel.2012.12.003

Choe, C. P., and Crump, J. G. (2014). Tbx1 controls the morphogenesis of pharyngeal pouch epithelia through mesodermal Wnt11r and Fgf8a. *Development* 141 (18), 3583–3593. doi:10.1242/dev.111740

Compagnucci, C., Martinus, K., Griffin, J., and Depew, M. J. (2021). Programmed cell death not as sledgehammer but as chisel: Apoptosis in normal and abnormal craniofacial patterning and development. *Front. Cell Dev. Biol.* 8 (9), 717404. doi:10.3389/fcell.2021.717404

Couly, G., Creuzet, S., Bennaceur, S., Vincent, C., and Le Douarin, N. M. (2002). Interactions between Hox-negative cephalic neural crest cells and the foregut endoderm in patterning the facial skeleton in the vertebrate head. *Development* 129 (4), 1061–1073. doi:10.1242/dev.129.4.1061

Crump, J. G., Maves, L., Lawson, N. D., Weinstein, B. M., and Kimmel, C. B. (2004). An essential role for Fgfs in endodermal pouch formation influences later craniofacial skeletal patterning. *Development* 131 (22), 5703–5716. doi:10.1242/dev.01444

Dahmann, C., and Basler, K. (1999). Compartment boundaries: At the edge of development. *Trends Genet.* 15 (8), 320–326. doi:10.1016/s0168-9525(99)01774-6

Depew, M. J., and Compagnucci, C. (2008). Tweaking the hinge and caps: Testing a model of the organization of jaws. *J. Exp. Zool. B Mol. Dev. Evol.* 310 (4), 315–335. doi:10.1002/jez.b.21205

Depew, M. J., Lufkin, T., and Rubenstein, J. L. (2002b). Specification of jaw subdivisions by Dlx genes. *Science* 298 (5592), 381–385. doi:10.1126/science.1075703

Depew, M. J., and Simpson, C. A. (2006). 21st century neontology and the comparative development of the vertebrate skull. *Dev. Dyn.* 235 (5), 1256–1291. doi:10.1002/dvdy.20796

Depew, M. J., Tucker, A., and Sharpe, P. (2002a). "Craniofacial development," in *Mouse development: Patterning, morphogenesis, and organogenesis*. Editors J. Rossant and P. Tam (London: Academic Press), 421–498.

Edlund, R. K., Ohyama, T., Kantarci, H., Riley, B. B., and Groves, A. K. (2014). Foxi transcription factors promote pharyngeal arch development by regulating formation of FGF signaling centers. *Dev. Biol.* 390 (1), 1–13. doi:10.1016/j.ydbio.2014.03.004

Ferguson, C. A., Tucker, A. S., and Sharpe, P. T. (2000). Temporospatial cell interactions regulating mandibular and maxillary arch patterning. *Development* 127 (2), 403–412. doi:10.1242/dev.127.2.403

Fish, J. L., Villmoare, B., Kobernick, K., Compagnucci, C., Britanova, O., Tarabykin, V., et al. (2011). Satb2, modularity, and the evolvability of the vertebrate jaw. *Evol. Dev.* 13 (6), 549–564. doi:10.1111/j.1525-142X.2011.00511.x

Frank, D. U., Fotheringham, L. K., Brewer, J. A., Muglia, L. J., Tristani-Firouzi, M., Capecchi, M. R., et al. (2002). An Fgf8 mouse mutant phenocopies human 22q11 deletion syndrome. *Development* 129 (19), 4591–4603. doi:10.1242/dev.129.19.4591

Gendron-Maguire, M., Mallo, M., Zhang, M., and Gridley, T. (1993). Hoxa-2 mutant mice exhibit homeotic transformation of skeletal elements derived from cranial neural crest. *Cell* 75 (7), 1317–1331. doi:10.1016/0092-8674(93)90619-2

Gower, J. C. (1975). Generalized procrustes analysis. *Psychometrika* 40, 33–51. doi:10.1007/bf02291478

Graham, A. (2003). Development of the pharyngeal arches. *Am. J. Med. Genet. A* 119A (3), 251–256. doi:10.1002/ajmg.a.10980

Graham, A., Okabe, M., and Quinlan, R. (2005). The role of the endoderm in the development and evolution of the pharyngeal arches. *J. Anat.* 207 (5), 479–487. doi:10.1111/j.1469-7580.2005.00472.x

Graham, A., and Smith, A. (2001). Patterning the pharyngeal arches. *Bioessays* 23 (1), 54–61. doi:10.1002/1521-1878(200101)23:1<54::AID-BIES1007>3.0.CO;2-5

Graham, A. (2001). The development and evolution of the pharyngeal arches. *J. Anat.* 199 (1-2), 133–141. doi:10.1046/j.1469-7580.2001.19910133.x

Green, R. M., Fish, J. L., Young, N. M., Smith, F. J., Roberts, B., Dolan, K., et al. (2017). Developmental nonlinearity drives phenotypic robustness. *Nat. Commun.* 8 (1), 1970. doi:10.1038/s41467-017-02037-7

Grevellec, A., and Tucker, A. S. (2010). The pharyngeal pouches and clefts: Development, evolution, structure and derivatives. *Semin. Cell Dev. Biol.* 21 (3), 325–332. doi:10.1016/j.semcdb.2010.01.022

Griffin, J. N., Compagnucci, C., Hu, D., Fish, J., Klein, O., Marcucio, R., et al. (2013). Fgf8 dosage determines midfacial integration and polarity within the nasal and optic capsules. *Dev. Biol.* 374 (1), 185–197. doi:10.1016/j.ydbio.2012.11.014

Hasten, E., and Morrow, B. E. (2019). Tbx1 and Foxi3 genetically interact in the pharyngeal pouch endoderm in a mouse model for 22q11.2 deletion syndrome. *PLoS Genet.* 15 (8), e1008301. doi:10.1371/journal.pgen.1008301

Haworth, K. E., Wilson, J. M., Grevellec, A., Cobourne, M. T., Healy, C., Helms, J. A., et al. (2007). Sonic hedgehog in the pharyngeal endoderm controls arch pattern via regulation of Fgf8 in head ectoderm. *Dev. Biol.* 303 (1), 244–258. doi:10.1016/j.ydbio.2006.11.009

Jackson, A., Kasah, S., Mansour, S. L., Morrow, B., and Basson, M. A. (2014). Endoderm-specific deletion of Tbx1 reveals an FGF-independent role for Tbx1 in pharyngeal apparatus morphogenesis. *Dev. Dyn.* 243 (9), 1143–1151. doi:10.1002/dvdy.24147

Jandzik, D., Hawkins, M. B., Cattell, M. V., Cerny, R., Square, T. A., and Medeiros, D. M. (2014). Roles for FGF in lamprey pharyngeal pouch formation and skeletogenesis highlight ancestral functions in the vertebrate head. *Development* 141 (3), 629–638. doi:10.1242/dev.097261

Jerome, L. A., and Papaioannou, V. E. (2001). DiGeorge syndrome phenotype in mice mutant for the T-box gene, Tbx1. *Nat. Genet.* 27 (3), 286–291. doi:10.1038/85845

Kindberg, A. A., and Bush, J. O. (2019). Cellular organization and boundary formation in craniofacial development. *Genesis* 57 (1), e23271. doi:10.1002/dvg.23271

Kitazawa, T., Takechi, M., Hirasawa, T., Adachi, N., Narboux-Neme, N., Kume, H., et al. (2015). Developmental genetic bases behind the independent origin of the tympanic membrane in mammals and diapsids. *Nat. Commun.* 6, 6853. doi:10.1038/ncomms7853

Kuratani, S. (2012). Evolution of the vertebrate jaw from developmental perspectives. *Evol. Dev.* 14 (1), 76–92. doi:10.1111/j.1525-142X.2011.00523.x

Macatee, T. L., Hammond, B. P., Arenkiel, B. R., Francis, L., Frank, D. U., and Moon, A. M. (2003). Ablation of specific expression domains reveals discrete functions of ectoderm- and endoderm-derived FGF8 during cardiovascular and pharyngeal development. *Development* 130 (25), 6361–6374. doi:10.1242/dev.00850

Meyers, E. N., Lewandoski, M., and Martin, G. R. (1998). An Fgf8 mutant allelic series generated by Cre- and Flp-mediated recombination. *Nat. Genet.* 18 (2), 136–141. doi:10.1038/ng0298-136

Moon, A. M., Guris, D. L., Seo, J. H., Li, L., Hammond, J., Talbot, A., et al. (2006). Crkl deficiency disrupts Fgf8 signaling in a mouse model of 22q11 deletion syndromes. *Dev. Cell* 10 (1), 71–80. doi:10.1016/j.devcel.2005.12.003

Okubo, T., Kawamura, A., Takahashi, J., Yagi, H., Morishima, M., Matsuoka, R., et al. (2011). Ripply3, a Tbx1 repressor, is required for development of the pharyngeal apparatus and its derivatives in mice. *Development* 138 (2), 339–348. doi:10.1242/dev.054056

Park, E. J., Ogden, L. A., Talbot, A., Evans, S., Cai, C. L., Black, B. L., et al. (2006). Required, tissue-specific roles for Fgf8 in outflow tract formation and remodeling. *Development* 133 (12), 2419–2433. doi:10.1242/dev.02367

Piotrowski, T., Ahn, D. G., Schilling, T. F., Nair, S., Ruvinsky, I., Geisler, R., et al. (2003). The zebrafish van gogh mutation disrupts tbx1, which is involved in the DiGeorge deletion syndrome in humans. *Development* 130 (20), 5043–5052. doi:10.1242/dev.00704

Piotrowski, T., and Nusslein-Volhard, C. (2000). The endoderm plays an important role in patterning the segmented pharyngeal region in zebrafish (*Danio rerio*). *Dev. Biol.* 225 (2), 339–356. doi:10.1006/dbio.2000.9842

Poopalasundaram, S., Richardson, J., Scott, A., Donovan, A., Liu, K., and Graham, A. (2019). Diminution of pharyngeal segmentation and the evolution of the amniotes. *Zool. Lett.* 5, 6. doi:10.1186/s40851-019-0123-5

Pujades, C. (2020). The multiple functions of hindbrain boundary cells: Tinkering boundaries? *Semin. Cell Dev. Biol.* 107, 179–189. doi:10.1016/j.semcdb.2020.05.002

Que, J., Okubo, T., Goldenring, J. R., Nam, K. T., Kurotani, R., Morrisey, E. E., et al. (2007). Multiple dose-dependent roles for Sox2 in the patterning and differentiation of anterior foregut endoderm. *Development* 134 (13), 2521–2531. doi:10.1242/dev.003855

Quinlan, R., Gale, E., Maden, M., and Graham, A. (2002). Deficits in the posterior pharyngeal endoderm in the absence of retinoids. *Dev. Dyn.* 225 (1), 54–60. doi:10.1002/dvdy.10137

Quinlan, R., Martin, P., and Graham, A. (2004). The role of actin cables in directing the morphogenesis of the pharyngeal pouches. *Development* 131 (3), 593–599. doi:10.1242/dev.00950

Rijli, F. M., Mark, M., Lakkaraju, S., Dierich, A., Dolle, P., and Chambon, P. (1993). A homeotic transformation is generated in the rostral branchial region of the head by disruption of Hoxa-2, which acts as a selector gene. *Cell* 75 (7), 1333–1349. doi:10.1016/0092-8674(93)90620-6

Rohlf, J. S. D., and Slice, D. (1990). Extensions of the procrustes method for the optimal superimposition of landmarks. *Syst. Biol.* 39 (1), 40–59. doi:10.2307/2992207

Sato, T., Kurihara, Y., Asai, R., Kawamura, Y., Tonami, K., Uchijima, Y., et al. (2008). An endothelin-1 switch specifies maxillomandibular identity. *Proc. Natl. Acad. Sci. U. S. A.* 105 (48), 18806–18811. doi:10.1073/pnas.0807345105

Shigetani, Y., Sugahara, F., Kawakami, Y., Murakami, Y., Hirano, S., and Kuratani, S. (2002). Heterotopic shift of epithelial-mesenchymal interactions in vertebrate jaw evolution. *Science* 296 (5571), 1316–1319. doi:10.1126/science.1068310

Shone, V., and Graham, A. (2014). Endodermal/ectodermal interfaces during pharyngeal segmentation in vertebrates. *J. Anat.* 225 (5), 479–491. doi:10.1111/joa.12234

Trainor, P. A., and Krumlauf, R. (2001). Hox genes, neural crest cells and branchial arch patterning. *Curr. Opin. Cell Biol.* 13 (6), 698–705. doi:10.1016/s0955-0674(00)00273-8

Trumpp, A., Depew, M. J., Rubenstein, J. L., Bishop, J. M., and Martin, G. R. (1999). Cre-mediated gene inactivation demonstrates that FGF8 is required for cell survival and patterning of the first branchial arch. *Genes Dev.* 13 (23), 3136–3148. doi:10.1101/gad.13.23.3136

Tsuchiya, Y., Mii, Y., Okada, K., Furuse, M., Okubo, T., and Takada, S. (2018). Ripply3 is required for the maintenance of epithelial sheets in the morphogenesis of pharyngeal pouches. *Dev. Growth Differ.* 60 (2), 87–96. doi:10.1111/dgd.12425

Tucker, A. S., Matthews, K. L., and Sharpe, P. T. (1998). Transformation of tooth type induced by inhibition of BMP signaling. *Science* 282 (5391), 1136–1138. doi:10.1126/science.282.5391.1136

Van Otterloo, E., Milanda, I., Pike, H., Thompson, J. A., Li, H., Jones, K. L., et al. (2022). AP-2α and AP-2β cooperatively function in the craniofacial surface ectoderm to regulate chromatin and gene expression dynamics during facial development. *Elife* 11, e70511. doi:10.7554/eLife.70511

Veitch, E., Begbie, J., Schilling, T. F., Smith, M. M., and Graham, A. (1999). Pharyngeal arch patterning in the absence of neural crest. *Curr. Biol.* 9 (24), 1481–1484. doi:10.1016/s0960-9822(00)80118-9

Vitelli, F., Morishima, M., Taddei, I., Lindsay, E. A., and Baldini, A. (2002a). Tbx1 mutation causes multiple cardiovascular defects and disrupts neural crest and cranial nerve migratory pathways. *Hum. Mol. Genet.* 11 (8), 915–922. doi:10.1093/hmg/11.8.915

Vitelli, F., Taddei, I., Morishima, M., Meyers, E. N., Lindsay, E. A., and Baldini, A. (2002b). A genetic link between Tbx1 and fibroblast growth factor signaling. *Development* 129 (19), 4605–4611. doi:10.1242/dev.129.19.4605

Zbasnik, N., Dolan, K., Buczkowski, S. A., Green, R. M., Hallgrimsson, B., Marcucio, R. S., et al. (2022). Fgf8 dosage regulates jaw shape and symmetry through pharyngeal-cardiac tissue relationships. *Dev. Dyn.* 251, 1711–1727. doi:10.1002/dvdy.501

Zhang, Z., Cerrato, F., Xu, H., Vitelli, F., Morishima, M., Vincentz, J., et al. (2005). Tbx1 expression in pharyngeal epithelia is necessary for pharyngeal arch artery development. *Development* 132 (23), 5307–5315. doi:10.1242/dev.02086

Zhang, Z., Huynh, T., and Baldini, A. (2006). Mesodermal expression of Tbx1 is necessary and sufficient for pharyngeal arch and cardiac outflow tract development. *Development* 133 (18), 3587–3595. doi:10.1242/dev.02539